

Trojan-Resilient NTT: Protecting Against Control Flow and Timing Faults on Reconfigurable Platforms

Rourab Paul¹, Krishnendu Guha², Amlan Chakrabarti³

Dept. of Computer Science and Engineering, Shiv Nadar University, Chennai, Tamil Nadu, India¹

School of Computer Science and Information Technology, University College Cork, Ireland²

School of IT, University of Calcutta, West Bengal, India³

rourabpaul@snuchennai.edu.in¹, kgguha@ucc.ie², acakcs@caluniv.ac.in³

Abstract—Number Theoretic Transform (NTT) is the most essential component for polynomial multiplications used in lattice-based Post-Quantum Cryptography (PQC) algorithms such as Kyber, Dilithium, NTRU etc. However, side-channel attacks (SCA) and hardware vulnerabilities in the form of hardware Trojans may alter control signals to disrupt circuit’s control flow and introduce unconventional delays in the critical hardware of PQC. Hardware Trojans, especially on control signals, are more low cost and impactful than data signals because a single corrupted control signal can disrupt or bypass entire computation sequences, whereas data faults usually cause only localized errors. On the other hand, adversaries can perform Soft Analytical Side Channel Attacks (SASCA) on the design using the inserted hardware Trojan. In this paper, we present a secure NTT architecture capable of detecting unconventional delays, control-flow disruptions, and SASCA, while providing an adaptive fault-correction methodology for their mitigation. Extensive simulations and implementations of our Secure NTT on Artix-7 FPGA with different Kyber variants show that our fault detection and correction modules can efficiently detect and correct faults whether caused unintentionally or intentionally by hardware Trojans—with a high success rate, while introducing only modest area and time overheads.

Index Terms—Side Channel Attack, Hardware Trojan, SASCA, NTT, Control Flow Integrity.

I. INTRODUCTION

The NTT significantly reduces the time complexity of multiplying degree- $n - 1$ polynomials from $\mathcal{O}(n^2)$ to $\mathcal{O}(n \log n)$. As a result, standardized lattice-based PQC schemes such as Kyber, Dilithium, and NTRU benefit from substantial acceleration across various secure processing platforms. This acceleration of PQCs [1], [2], [3] in FPGA makes them suitable for future high-speed data communication infrastructure. However, NTT suffers from side-channel attacks [4] and other hardware Trojans [5] that may reveal multiple secret shares during NTT computation. A hardware Trojan [6] can deliberately induce controlled side-channel leakages like SASCA [7], [8]. The growing demand for FPGAs in defense, aerospace, automotive, and telecommunications is projected to reach 11 billion USD [9] by 2027. This rising popularity has globalized the FPGA supply chain, thereby increasing the risk of hardware Trojans in modern systems. Consequently, the attack surface for

hardware Trojan insertion has expanded across multiple stages, including RTL [10], synthesis [11], or foundry stages. Moreover, hardware Trojans can also be inserted after bit-stream generation [12]. The variety of Trojan insertion stages and the diverse nature of hardware Trojans mainly target the data signals and control signals of the system. However, attackers mostly [13] prefer inserting Trojans into control signals due to their low cost and high impact. For example, gating the clock, flipping the reset, or delaying the enable signal can stall or misdirect the entire datapath and disrupt the control flow.

A. Threat Models

In FPGA fabric, vulnerabilities can arise intentionally or unintentionally. Unintentional vulnerabilities may result from aging that may cause performance degradation and excessive power consumption over time. Additionally, adversaries present in third-party design houses may intentionally insert hardware Trojans into the FPGA fabric (design-time or foundry-level) or bitstream (post-design, deployment-time). Hardware Trojans may be introduced into the system through compromised CAD tools [14]. A malicious CAD tool could bypass or neutralize testing and post-silicon validation [15]. Trojans can also be inserted during deployment by tampering with the bitstream [12]. On the other hand, without any modification of the design, purely observational attacks such as SASCA [7], [8] can be extremely powerful against cryptographic systems if is unprotected. All these attack phases may affect the integrity, confidentiality and availability of the crypto system. In this work, we focus on hardware vulnerabilities that cause unconventional delays, disrupt the expected behavior (Control Flow) of the hardware, cause information leakage, produce erroneous outputs and degrade overall circuit performance. If the proposed Secure NTT is part of a malicious bitstream, or placed in an infected FPGA fabric, or subjected to aged or heated FPGA conditions, any unconventional delays or abnormal control flow in the NTT caused by these factors can be detected.

B. Literature

The existing literature on NTT can broadly be categorized into two directions. The first line of work focuses primarily on optimizing NTT implementations for ASICs, FPGAs, and embedded processors [2], [1], [3]. In contrast, another body of research addresses the protection of NTT against hardware Trojans and side-channel attacks such as SASCA. Prior works on protected NTT have mainly proposed fault-detection mechanisms, targeting either data signals or control signals.

1) *Protection on Data Signals of NTT*: To protect the data signals of the NTT, it is necessary to secure the arithmetic operations of the NTT, since these operations are the source of the data. As shown in Algorithm 1, the main data signals of the NTT involve the computation of V through polynomial multiplication followed by modular reduction, as well as the memory addresses j and k used to access the coefficient memory and twiddle-factor memory, respectively. Article [16] proposed a fault detection module for NTT which targets the polynomial multiplication process of the NTT. They recomputed the multiplication result using the Recomputation with Negate Operands (RENO) technique on Spartan-6 and Zynq UltraScale+ platforms, incurring a 12.74% resource overhead and approximately 20% power overhead. The proposed RENO technique can detect errors in $A[k1]$ and ω (Line 11 of Algorithm 1) during the polynomial multiplication and reduction operations. Similarly, [17] presents a fault-detection model for the same V computation using Recomputation with Modular Offset (REMO), combined with a word-wise Montgomery reduction, implemented on an Artix-7 FPGA with an 8.5% slice overhead and a 1.8% energy overhead. They identified a correlation among the indices i , j , and k (Algorithm 1), which generate the memory addresses for polynomial coefficients and twiddle factors memories in each NTT iteration (Algorithm 1). This correlation-based method can detect hardware Trojans inserted in the memory address generation logic. Article [18] has also targeted Montgomery Reduction of the NTT using Recomputation based Shifted Operand (RESO). Sven et al. [19] target the data signals of the NTT, employing interpolation, evaluation, and inverse NTT techniques to detect faults in the multiplication with twiddle factors and the addition operations on the ARM Cortex-M4 platform.

2) *Protection on Control Signals of NTT*: Except for the aforementioned fault occurrences on data signals of the NTT, some works in the literature address control-flow and delay attacks caused by disruptions of the NTT control signals. Jati et al. [5] implemented a configurable CRYSTALS-Kyber architecture that addresses circuit delay and control flow integrity (*CFI*) violations caused by hardware Trojans inserted in control signals. This design includes the NTT, employs a duplicate inverted logic state machine to verify the Finite State Machine (FSM) of the Kyber processor and utilizes a Clock Cycle Counter (*CCC*) in the instruction module to detect unconventional delays in the entire crypto

processor. Since SCA can also be induced by hardware Trojans, several recent works have exploited power and timing leakages in NTT for lattice-based PQC, particularly SASCA attacks, using probabilistic models [4], [20]. To prevent SCAs on the NTT, Jati et al. [5] randomized memory addresses for each butterfly layer instead of using a linear increment in the memory address. This is possible because the order of NTT operation does not matter in a single butterfly layer. Article [7] also implemented the same memory address randomization technique for NTT to prevent side-channel attacks on the ARM Cortex-M4 platform. Additionally, it applied input masking using twiddle factors to protect NTT against SASCA. Rafael et al. [8] adopted the same input masking technique using twiddle factors in the NTT on a reconfigurable platform. However, instead of masking all inputs, they selectively masked only a subset and varied the number of masked inputs to observe the effect on power consumption.

To the best of our knowledge, our **Secure NTT** is the first design to detect hardware Trojan-based control-signal attacks, prevent unconventional delays and control-flow disruptions, and mitigate SASCA through local masking, while applying fault-specific adaptive correction measures. It should be noted that our **Secure NTT** does not perform fault detection or correction on data signals, unlike the approaches in [19], [16], [18] and [17]. The contributions of our article are summarized as :

- Unlike conventional duplicate Control Status Registers (CSR), we introduce a lightweight shift-register-based backup CSR, fully independent of the NTT logic, to verify and ensure Control Flow Integrity (*CFI*) in the NTT. Our adopted Clock Cycle Counter (*CCC*) mechanism safeguards all critical control and status signals against unintended delays. The input masking of polynomial coefficients with the twiddle factors in our NTT can prevent SASCA.
- The proposed adaptive fault-correction mechanism for FPGA-based designs utilizes multiple backups of partial (PR) bitstreams corresponding to different FPGA floor regions. Our proposed fault correction algorithm evaluates a risk factor (R_i) for each PR bitstreams corresponding to the FPGA floors of all critical components available in a system. Based on this R_i and the nature of the detected faults, it applies appropriate countermeasures. We implemented this adaptive fault correction methods for our NTT to dynamically respond to the specific nature of each detected fault, ensuring resilient operation against diverse hardware Trojan effects
- The proposed **Secure NTT** is implemented on an Artix-7 FPGA with 5 pipeline stages without incurring any timing overhead in fault detection. The implementation overhead of our fault detection and correction modules is minimal and competitive with existing NTT solutions.

The organization of this paper is described as follows. Sec-

tion II discusses our fault detection methods. The working principle of our fault correction methods is discussed in Section III. The Results of the implementation, conclusions and future scopes are presented in Section IV, Section V and VI respectively.

II. FAULT DETECTION MODULES

NTT primarily consists of 3 operations: memory read, arithmetic operations (mult, add, sub, modulus) and memory write. In our fault detection model, arithmetic operations in the NTT are masked using Local Masking (*LM*) at each clock cycle, while unintentional delays and control-flow integrity issues are addressed using the Clock Cycle Counter (*CCC*) and Control Flow Integrity (*CFI*), respectively.

Algorithm 1 NTT Algorithm

```

1: Input:  $A(x), \omega, q$ 
2: Output:  $\bar{A}(x)$ 
3:  $hl = \frac{n}{2}$ 
4: for  $i = 0$  to  $\log_2(n) - 1$  do
5:   for  $j = 0$  to  $2^i - 1$  do
6:     for  $k = 0$  to  $hl - 1$  do
7:        $\omega_j = \omega[j]$ 
8:        $k0 = k$ 
9:        $k1 = k + hl$ 
10:       $U = A[k0]$ 
11:       $V = (A[k1] \times \omega_j) \% q$ 
12:       $\bar{A}[k0] = (U + V) \% q$ 
13:       $\bar{A}[k1] = (U - V) \% q$ 
14:       $hl = \frac{hl}{2}$ 
15: return  $\bar{A}$ 

```

A. Control Flow Integrity

The proposed NTT includes 8 subcomponents (Table I); among them, only the *Bit Reverser* and *w_mem* operate without control signals. The remaining 6 use control signals for activation/reset and status signals like *done* or *ready* to indicate output readiness. This structured signaling framework ensures seamless coordination and efficient data flow across the NTT architecture. The control Flow Integrity of proposed Secure NTT is maintained with 3 strategies.

1) *Control Status Register (CSR)*: All input control signals for the sub-components of the proposed Secure NTT are generated by a 4-bit Control Status Register (*CSR*) placed inside the *CTRL* unit. The bits in *CSR* change if the *rst* input of the *NTT* becomes low. The bits of *CSR* from χ^{th} clock cycle to $(\chi+1)^{\text{th}}$ clock cycle can be represented as:

$$CSR_{i-1}(\chi+1) = \begin{cases} CSR_i(\chi), & \text{if } 0 \leq i < \eta-2, \text{ for } \chi = 1, \dots, \log n \times \frac{n}{2} \\ CSR_i(\chi), & \text{if } i = \eta-1, \end{cases}$$

Here χ indicates the clock cycles which iterates from 1 to $\log n \times \frac{n}{2}$ for the *NTT* operation of $n-1$ degree polynomial. Therefore, the proposed *NTT* requires $\log n \times \frac{n}{2}$ clock

Sub components	CSR Signals	Remarks
<i>poly_mem</i>	<i>rd_en</i> , <i>wr_en</i> , <i>polymem_ce</i>	<i>poly_mem</i> stores polynomial coefficients, <i>rd_en</i> and <i>wr_en</i> are used to read write from/to <i>poly_mem</i> , <i>poly_mem_ce</i> is used to enable <i>poly_mem</i>
<i>CTRL</i>	<i>CTRL_rst</i>	<i>CTRL</i> generate all the required control signals of sub-components, <i>CTRL_rst</i> is used to initiate the address values for <i>poly_mem</i> and <i>w_mem</i>
<i>U Buffer</i>	<i>uBuff_rst</i>	<i>uv_add</i> and <i>uv_sub</i> needs <i>u</i> and <i>v</i> as inputs, <i>u</i> comes directly from <i>poly_mem</i> but <i>v</i> needs 2 clock cycles to generate from Barrett reduction. Therefore, <i>u</i> needs to buffer for 2 clock cycles. <i>uBuff_rst</i> is used to reset pipeline buffers which hold the value <i>u</i> until <i>v</i> computes in Barrett Reduction
<i>Barrett Reduction</i>	<i>barrett_rst</i> , <i>barrett strt</i> , <i>barrett done</i>	It compute $v \times \omega \bmod q$. <i>barrett_rst</i> is used initialized intermediate registers of barrett reduction, <i>barrett strt</i> is used to start the barrett reduction when data from <i>poly_mem</i> and <i>w_mem</i> are ready, <i>barrett done</i> starts <i>uv_adder</i> and <i>uv_sub</i> .
<i>uv_adder</i> & <i>uv_sub</i>	<i>uv_rst</i> , <i>uv strt</i>	This blocks are required to add and subtract <i>u</i> and <i>v</i> . <i>uv_rst</i> make <i>uv_adder</i> & <i>uv_sub</i> in reset condition, <i>uv strt</i> starts <i>uv_adder</i> & <i>uv_sub</i>
<i>Bit Reverser</i>	-	This combinational logic block is required to generate a reading address of ω from <i>w_mem</i> .
<i>w_mem</i>	-	This is a ROM to store ω and it is a combinational logic block

TABLE I: Components & CSR Signals of Our Secure NTT

cycles. Here, the i^{th} bit of *CSR* at the χ^{th} clock cycle, denoted as $CSR_i[\chi]$, shifts to the $(i-1)^{\text{th}}$ bit of *CSR*, i.e., $CSR_{i-1}[\chi+1]$, at the $(\chi+1)^{\text{th}}$ clock cycle. Therefore, this *CSR* behaves like a right shift register. The size of the *CSR* is 4 bits because the proposed Secure NTT has five pipeline stages as shown in Fig. 4. Once the *rst* signal is de-asserted, the first pipeline stage is activated, and the remaining four pipeline stages are controlled by the 4 bits of the *CSR*. In our case, $n = 256$ and the pipeline depth is $p = 5$. Therefore, the complete *NTT* operation requires $(\log n \times \frac{n}{2}) + (p - 1) = 1024 + 4 = 1028$ clock cycles. The algorithm 1 illustrates the NTT operation, where $A(x)$ is the input polynomial in coefficient form with $n = 256$ coefficients. The output $\bar{A}(x)$ represents the point-value form of $A(x)$, and ω denotes the twiddle factor. As shown in Fig. 1, the *CSR[3]* and *CSR[2]* bits are used to generate *rd_en* and *uBuff_rst* respectively. The *CSR[0]* is used for *wr_en* and *uv strt*. The other required *CSR* signals can be generated from *CSR* using below equations.

$$\begin{aligned} uv_rst &= \neg CSR[3], \\ barrett_strt &= CSR[1] \vee CSR[2], \\ barrett_rst &= \neg (CSR[1] \vee CSR[2]), \\ poly_me_ce &= CSR[0] \vee CSR[3] \end{aligned}$$

The reset inputs of *CTRL* and *uBuff* are *CTRL_rst* and *uBuff_rst* respectively which are directly generated from *rst* input of the *NTT*. Therefore, *CTRL_rst=rst* and *uBuff_rst=rst*. The *CSR* is the core of the entire *NTT*, controlling all sub components by generating the nec-

essary control signals. The timing diagram of the proposed NTT, along with all control and status signals, is shown in Fig. 3.

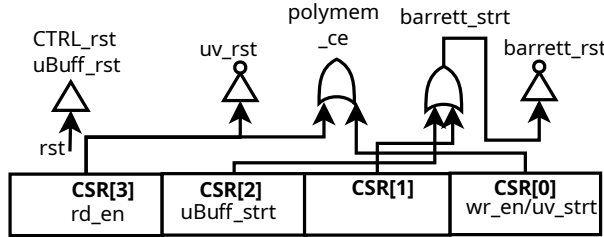


Fig. 1: Control and Status Signals of NTT



Fig. 2: Right Shift Register

2) *Right Shift Register (RSR)*: As shown in Fig. 3, it is observed that after *rst* of NTT goes low, *rd_en* (CSR[3]) becomes high. Subsequently, in the next three clock cycles, *uBuff_RST* (CSR[1]), CSR[2], and *wr_en* (CSR[3]), *uv_RST* are asserted with a one-clock-cycle delay between each signal. The above-mentioned control signals become high for $\frac{n}{2} \times \log n$. As shown in Fig. 2, to monitor the control flow integrity of our NTT, a Right Shift Register (*RSR*) is designed similarly to *CRS*. Unlike the duplicate *CSR* in [5], our *RSR* is independent of the main NTT logic. Thus, any tampering in the main logic affects the duplicate *CSR*, but not our *RSR*. The 3rd (msb) bit of this *RSR* becomes '0' if *rd_en* is '0', and it becomes '1' if *rd_en* is '1'. Here, the value of this *RSR* should match the value of the *CSR* register for the $\frac{n}{2} \times \log n$ clock cycles.

3) *CFI Fault Detector*: The *CFI* fault detector consists of the *RSR* and it computes four fault flags (1) *barrett_cfi_fault* for *Barrett*. (2) *polymem_cfi_fault* for *poly_mem*. (3) & (4) *uv_cfi_fault* for *uv_add* and *uv_sub*. The final *cfi_fault* is computed by performing an AND operation on the aforementioned four fault signals. *barrett_cfi_fault*: The control flow faults in the *barrett* block can be identified by analyzing the interrelationships between its input control signals (*barrett strt*, *barrett rst*) and output status signal (*barrett done*). In our NTT, the behavior of the *barrett* is considered normal if the following four strict conditions are satisfied: (i) The *barrett strt* control signal is inversely aligned with the *barrett rst* signal, i.e., *barrett strt* = *not barrett rst*. (ii) The *barrett* block activates one cycle after *rd_en* goes high (flagged by CSR[2]) and deactivates one cycle before *wr_en* goes low (flagged by CSR[1]). Therefore, *barrett strt*=CSR[1] OR CSR[2]. (iii) For the same arguments mentioned in (ii) *barrett strt*=RSR[1] OR RSR[2]. (iv) The *barrett* used in our **Secure NTT** has 2 pipeline stages. The *barrett done* transitions two cycles after *barrett strt*, aligning precisely with

CSR[0]/ *wr_en*. This alignment must hold during NTT operation.

barrett_cfi_fault = '0' when *barrett strt* =
NOT *barrett rst* AND (CSR[1] OR CSR[2] = '1') AND
(RSR[1] OR RSR[2] = '1') AND *barrett done* = *wr_en*

polymem_cfi_fault: The control flow integrity of *poly_mem* is considered normal if the control input signals *wr_en*, *rd_en* and *poly_mem_ce* are strictly aligned with corresponding bits of the *RSR*. The aforementioned control signals of *poly_mem* are generated from the *CSR*. (i) *wr_en*=CSR[0], (ii) *rd_en*=CSR[3] and (iii) *poly_mem_ce*=CSR[0] OR CSR[3].

polymem_cfi_fault = '0' when (*rd_en* = RSR[3]) \wedge
(*wr_en* = RSR[0]) \wedge (*poly_mem_ce* = RSR[0] \vee RSR[3])

uv_cfi_fault: The *uv_add* and *uv_sub* blocks are executed in parallel. The alignment of the *uv_RST* and *uv strt* input control signals for both *uv_add* and *uv_sub* is completely identical. Therefore, the proposed **Secure NTT** feeds a common *uv_RST* and *uv strt* control signal to both blocks. Here the *uv_RST*= NOT CSR[3] and *uv strt*=CSR[0].

uv_cfi_fault = '0' when (CSR[3]=RSR[3]) \wedge
(CSR[0] = RSR[0]) \wedge (*uv strt* = *not uv_RST*)

As shown in Fig. 5, the three *CFI* fault signals belonging to the *CSR* signals — *barrett_cfi_fault*, *polymem_cfi_fault*, and *uv_cfi_fault* — are connected to the *CFI* block to generate the final output signal, *cfi_fault*.

B. Clock Cycle Counter (CCC)

Our five-stage pipelined **Secure NTT** requires $(\log n \times \frac{n}{2}) + 4$ clock cycles. For $n = 1024$, our NTT requires 1028 clock cycles for the entire polynomial transformation. The active-high signals - *rd_en*, *wr_en*, *polymem_ce*, *barrett strt*, *barrett done*, and *uv strt* - must remain high or low for a correlated value of 1024 clock cycles, starting after *CTRL_RST* goes low. Our **Secure NTT** uses a Clock Cycle Counter (*CCC*) to ensure that the *Poly_mem*, *Barrett*, *uv_add*, and *uv_sub* modules operate for the correct number of clock cycles. Any unintentional or injected faults via hardware Trojans that cause additional clock-cycle delays in any of the aforementioned sub-components can be detected by the *CCC_fault* output (shown in Fig. 5) from the *CCC* module.

C. Local Mask (LM) Unit

To mitigate SASCA [4] on our **Secure NTT**, we employ local masking by randomizing the twiddle factors ω during the write operations to *poly_mem*. The availability of ω in *w_mem* makes this process convenient. As shown in Eq. 1, the *uv_adder* and *uv_sub* of the **Secure NTT** writes $\bar{A}[k0]$ and $\bar{A}[k1]$ in the *poly_mem* (Line 12 & Line 13 of Algorithm 1).

$$\bar{A}[k0] \leftarrow (U + V)\%q, \bar{A}[k1] \leftarrow (U - V)\%q \quad (1)$$

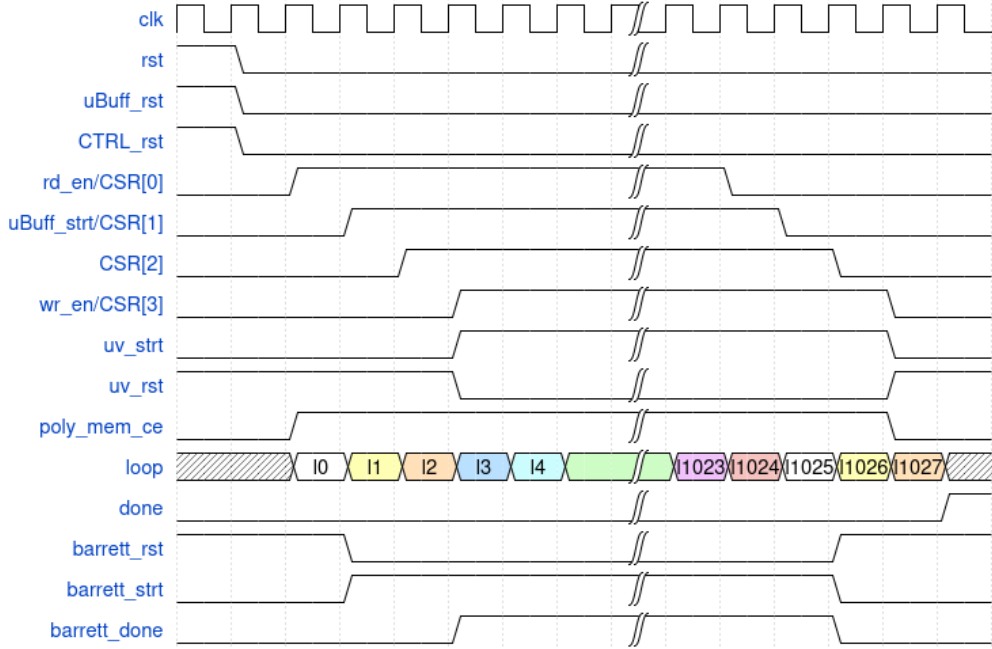


Fig. 3: Timing Diagram of Our Secure NTT

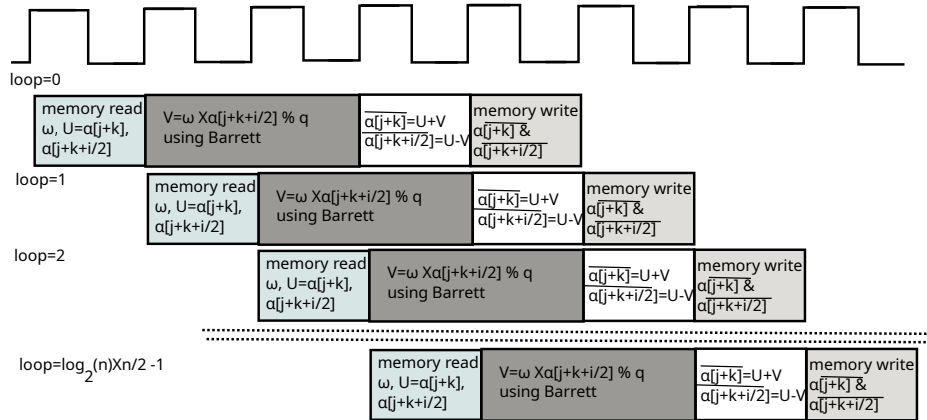


Fig. 4: Pipeline Stages of proposed Secure NTT

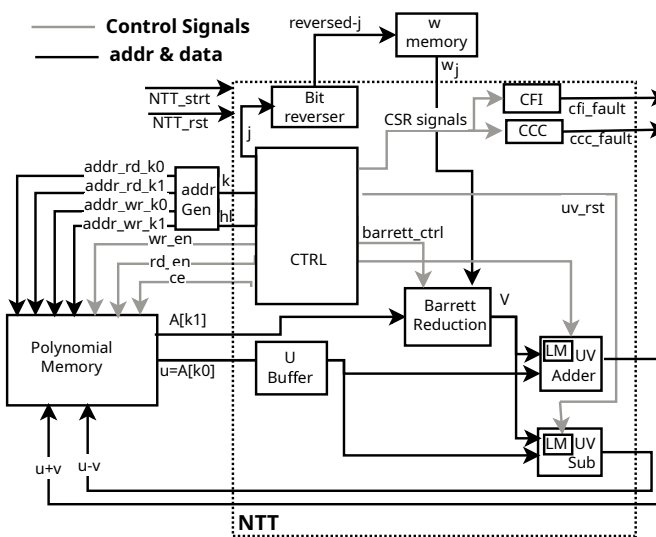


Fig. 5: Architecture of Secure NTT with Fault Detection Module

$$\bar{A}[k0] \leftarrow (U + V)\omega_r \% q, \bar{A}[k1] \leftarrow (U - V)\omega_r \% q \quad (2)$$

Instead of Eq. 1, we compute Eq. 2 within the *LM* units of *uv_adder* and *uv_sub* during the *poly_mem* write operation. Here ω_r is a random twiddle factor available in *w_mem*. In inverse NTT, we again multiply ω_r^{-1} available in *w_mem* to get the original polynomial coefficients.

III. ADAPTIVE FAULT CORRECTION MODULE

Our adaptive fault correction methods in NTT, generates m PR bitstream files for the same NTT architecture placed at different locations on the FPGA floor. For example, PR_1 corresponds to NTT_1 , PR_2 corresponds to NTT_2 , and so on, up to PR_m for NTT_m .

A. Measures

If *cfi_fault* or *ccf_fault* occurs, the Secure NTT can perform three types of measures in our architecture:

1) *Repeat Previous Loop*: If a fault is detected in an FPGA, migrating the hardware task to a different FPGA floor or reconfiguring it with a new bitstream is a widely adopted technique. However, hardware task migration, often termed a context switch of the hardware task, is very expensive in terms of timing overhead [21]. Therefore, splitting the NTT flow at specific boundaries or nodes can reduce the context-switching overhead of hardware tasks. Our Secure NTT supports fine-grained splitting at each clock cycle. If the fault is detected, the *results* ($U + V$ and $U - V$) of the previous NTT iteration can be discarded and the loop can be re-executed using the same ω_j from w_mem and $A[k0]$ and $A[k1]$ from $poly_mem$ (addressed by j and k respectively) with the same PR bitstream file of the NTT.

2) *Reload PR Bit & Repeat Previous Loop*: The same PR bitstream of the NTT can be reloaded in the same location of the FPGA floor with the help of Internal Configuration Access Port (ICAP) and repeat measure III-A1.

3) *Relocate PR Bit & Repeat Previous Loop*: The location of the NTT on the FPGA floor can be relocated by using different PR bitstream files of the NTT with the ICAP and repeat measure III-A1.

It is to be noted that hardware task context switching requires both reading and writing of bitstreams, whereas splitting the NTT flow eliminates the bitstream reading step, making III-A2 and III-A3 more lightweight compared to conventional context switching. The above-mentioned measures are taken based on two thresholds for the *cfi_fault* and the *ccc_fault* occurrence. For *cfi_fault*, the threshold values are defined as *cfi_th_reld* and *cfi_th_relc*. As shown in line 9 of Algorithm 2, if the *cfi_fault* count (*ncfi_fault*) exceeds *cfi_th_reld* but remains below *cfi_th_relc*, then measure III-A2 is applied. As shown in line 12 of Algorithm 2, if *ncfi_fault* exceeds *cfi_th_relc*, then measure III-A3 is applied. This check on *ncfi_fault* is performed in every NTT loop iteration during each clock cycle. After completing an NTT iteration, the same procedure is applied to *ccc_fault*. These steps are detailed in lines 20–27 of Algorithm 2. To incorporate measures III-A1, III-A2 and III-A3, our fault correction module introduces three additional components into the NTT architecture.

B. Bit Patcher

The bit patcher is an application that runs on the host CPU. The primary responsibility of our bit patcher is to manage the PR bitstreams of the NTT. Depending on the required measures, it may reconfigure the same PR bitstream or, in some cases, load a different PR bitstream of the NTT. When a different bitstream is required, our bit patcher selects it based on a risk factor (R_i).

1) *R_i Calculation*: The value of R_i is calculated based on the number and types of faults that are considered for the system. Suppose a total of ϕ fault types are considered, denoted by F_1, F_2, \dots, F_ϕ , with corresponding weights $W_{F_1}, W_{F_2}, \dots, W_{F_\phi}$. For any i^{th} PR bit stream PR_i of a component or core, let the number of F_1 -type faults be nF_{1j} ,

Algorithm 2 Fault Correction of NTT

```

1: Input:  $A(x), \omega, q$ 
2: Output:  $\bar{A}(x)$ 
3:  $hl = \frac{n}{2}$ 
4: for  $i = 0$  to  $\log_2(n) - 1$  do
5:   for  $j = 0$  to  $2^i - 1$  do
6:     for  $k = 0$  to  $hl - 1$  do
7:       if cfi_fault
8:         ncfi_fault ++
9:         if (ncfi_fault > cfi_th_reld) &
10:            (ncfi_fault < cfi_th_relc)
11:              Reload PR bit
12:              Repeat Previous Loop
13:            else if ncfi_fault > cfi_th_relc
14:              Relocate PR bit
15:              Repeat Previous Loop
16:            else
17:              Repeat Previous Loop
18:       if ccc_fault
19:         nccc_fault ++
20:         if (nccc_fault > ccc_th_reld) &
21:            (nccc_fault < ccc_th_relc)
22:              Reload PR bit
23:              Repeat Previous Loop
24:            else if nccc_fault > ccc_th_relc
25:              Relocate PR bit
26:              Repeat Previous Loop
27:            else
28:              Repeat Previous Loop
29: return  $\bar{A}$ 

```

the number of F_2 -type faults be nF_{2j} , and so on. If the total number of runs for the i^{th} component or core is NR_i , then the expression for calculating R_i can be written as:

$$R_i = \sum_{j=1}^{\phi} W_{F_j} \cdot \frac{nF_{j/NR_j}}{\max_n F_{jk}/NR_k} \quad (3)$$

Here, $\max_n F_{jk}$ denotes the maximum number of F_j -type fault occurrences for the PR bitstream PR_k in the FPGA floor F_k , and NR_k represents the number of runs of the PR bitstream PR_k . The value of k will be different for each loop of j . It is possible that a particular PR bitstream of a component or core is selected by the bit patcher more frequently than others. Consequently, a component or core that is invoked more often is also likely to exhibit a higher absolute number of fault occurrences, not necessarily because it is more fault-prone but simply due to its higher utilization. To mitigate this bias, we normalize the raw fault counts by the number of times each component or core is selected. Specifically, instead of directly using nF_j , we consider the normalized quantities $\max_n F_{jk}/NR_k$. The same normalization is also required in the denominator of Eq. 3, where the maximum numbers of nF_j faults occur in k^{th} core or component. Without this adjustment, the

denominator would similarly be biased by the number of times a particular core or component is selected.

The $\sum_{j=1}^{\phi} W_{F_j} = 1$. If R_i is the same for two PR bitstreams, the bit patcher selects the PR bitstream with the higher number of runs.

2) R_i Calculation for Secure NTT: In our Secure NTT, we considered only two types of faults: *cfi_fault* and *ccc_fault*; therefore, $\phi = 2$. Therefore, our bit patcher collects the number of *cfi_fault* and *ccc_fault* occurrences from all m available NTTs in our architecture. Note that only one NTT is active at a time, while the remaining $m - 1$ NTTs are blank, meaning their PR bitstreams are not configured. The bit patcher application profiles the m NTTs based on the number of *cfi_fault* and *ccc_fault* occurrences, and computes a risk factor R_i for each NTT. Based on the calculated R_i values, the bit patcher selects the appropriate PR bitstream during measure III-A3 only. We have m PR bitstreams $\{PR_1, PR_2, \dots, PR_m\}$ for $\{NTT_1, NTT_2, \dots, NTT_m\}$ mapped to FPGA floors $\{f_1, f_2, \dots, f_m\}$. Each PR_i exhibits runtime fault counts: $ncfi_fault_i$, representing the number of *cfi_fault* occurrences, and $nccc_fault_i$, representing the number of *ccc_fault* occurrences for NTT_i , where $i \in 1, 2, \dots, m$. In the R_i calculation for NTT_i , $ncfi_fault_i$ and $nccc_fault_i$ are normalized by dividing them by $\max_{j} ncfi_fault_j$ and $\max_k nccc_fault_k$, respectively. Here, it is assumed that in NTT_j and NTT_k , our proposed fault detection module detects the maximum number of *cfi_fault* and *ccc_fault*, respectively. The $\max_{j} ncfi_fault_j$ denotes the maximum number of *cfi_faults* detected in NTT_j and $\max_k nccc_fault_k$ represents maximum number of *ccc_faults* detected in NTT_k . The objective of the bit patcher is to select the PR file with minimal risk where risk R_i depends on both $ncfi_fault_i$ and $nccc_fault_i$. We redefine a composite risk factor R_i for PR_i bitstream as

$$R_i = W_{cfi} \cdot \frac{ncfi_fault_i}{NR_i} + W_{ccc} \cdot \frac{nccc_fault_i}{NR_i} \quad (4)$$

Here W_{cfi} and W_{ccc} are weights which reflects the relative

	NR	$ncfi_fault$	$nccc_fault$	R
NTT_1				
NTT_2				
.....				
NTT_m				

Fig. 6: Bit Patcher Table

importance of control-flow faults cfi_fault_i and unconventional delays fault ccc_fault_i of i^{th} NTT which is known as NTT_i . If control-flow faults cfi_fault are more critical, set $W_{cfi} > W_{ccc}$. If unconventional delays fault ccc_fault are more critical, set $W_{ccc} > W_{cfi}$. In our system, we use $W_{cfi} = 0.5$ and $W_{ccc} = 0.5$. For the relocation of the NTT in measure III-A3, the bit patcher selects the PR_i bitstream of NTT_i that has the minimum risk score R_i . As shown in

Fig. 6, the bit patcher maintain a table which store number of runs (NR), $ncfi_fault$, $nccc_fault$ and R for each NTT.

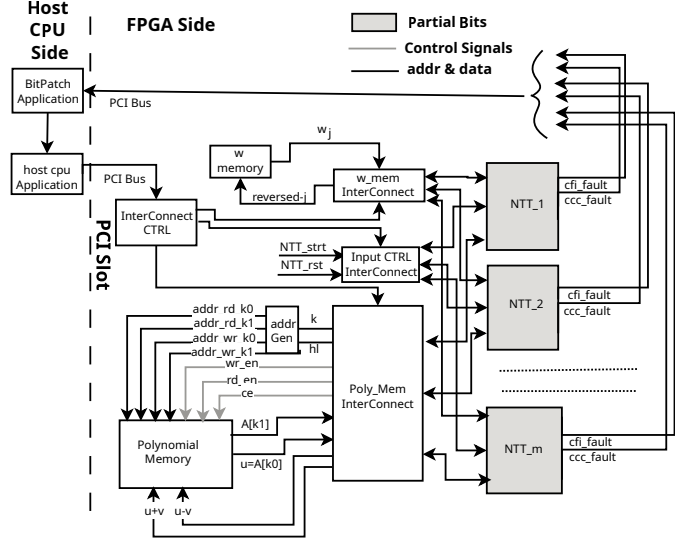


Fig. 7: Architecture of Secure NTT With Fault Correction Module

C. Bus Inter Connects

Except for the clock input, our NTT module has four inputs: NTT_rst , NTT_strt , $A[k0]$, and $A[k1]$, and eight outputs: j , k , hl , rd_en , wr_en , ce , $U + V$, and $U - V$. The NTT only interacts with *poly_mem* and *w_mem*. Our fault correction methods allow a fresh NTT to be loaded in a different FPGA floor. For this reason, we define multiple NTT instances across FPGA floors. Whenever a new NTT is loaded, it must be connected to *poly_mem* and *w_mem*. Therefore, the connections between *poly_mem*, *w_mem*, and the NTT must be dynamic. To achieve this, we create three bus interconnects that link control inputs (NTT_rst , NTT_strt), *poly_mem* and *w_mem* to the currently active NTT. At any given time, only one NTT is active, while the remaining NTTs remain unconfigured (their PR bitstreams are not loaded). In our fault detection method, we use three bus interconnects: (i) *poly_mem InterConnects*, which connects *poly_mem* to the selected NTT, (ii) *w_mem InterConnects*, which connects *w_mem* to the selected NTT, and (iii) *Input CTRL InterConnects*, which connects the control inputs (NTT_rst , NTT_strt) to the selected NTT. Whenever bitpatcher relocate NTT in different FPGA floor, bit patcher configures the bus interconnects using the *InterConnect CTRL*. For all three bus interconnects, we use a buffer to store the previous values. This is necessary because if a fault is detected, the NTT must recompute the previous loops using these buffered values. The proposed Secure NTT along with the fault correction module is shown in Fig. 7. The *addr_gen* takes k and hl from NTT and generate read and write addresses of *poly_mem*.

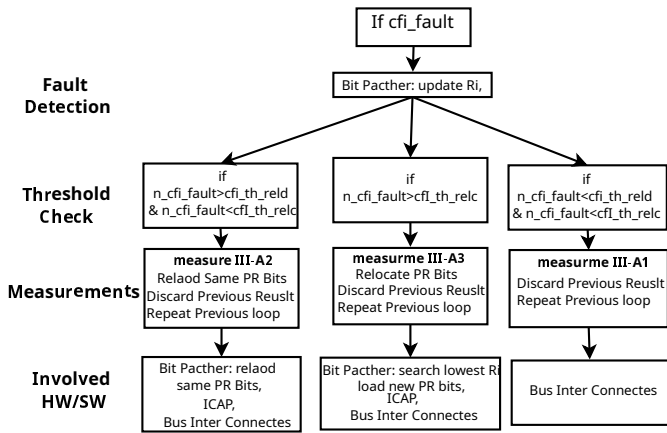


Fig. 8: Flow Diagram of Fault Correction Module for *cfi_fault*

D. Fault Correction Flow

Whenever the proposed *cfi_fault* and *ccc_fault* mechanisms detect faults, they update the fault counts to the bit patcher, which consequently updates the R_i of the corresponding NTT block. Thereafter, three conditions stated in Algorithm 2 are checked based on four thresholds: *cfi_th_reld*, *cfi_th_relc*, *ccc_th_reld*, and *ccc_th_relc*. The three conditions for *cfi_fault* occurrences, shown in line 9 as measure III-A2, line 12 as measure III-A3, and line 15 as measure III-A1 of Algorithm 2, trigger the three types of fault corrections implemented in our **Secure NTT**. The proposed fault correction module involves only the bus interconnects (stated in Sec. III-C) for measure III-A1. It involves reloading same PR bit step of bit patcher, ICAP [22] and bus interconnects for measure III-A2. Finally for measure III-A3, it involves searching for lowest R_i NTT, download new PR bit steps of Bit patcher, ICAP and bus interconnects. Fig. 8 shows the four steps that are performed following the detection of a *cfi_fault*. Depending on the three types of measures, the hardware and software components involved in each step differ accordingly. The same sequence of steps is also applied when a *ccc_fault* is detected.

IV. IMPLEMENTATION & RESULTS

As depicted in Fig. 7, the proposed **Secure NTT** architecture is implemented on an Artix-7 FPGA using VHDL and the Vivado 2022.2 tool. The host side code is written in C. The NTT is placed inside FPGA is connected with a *i5* host CPU through PCI bus.

A. Our Validation Strategies

To validate our fault detection and correction methods, we implemented three variants of Kyber (Kyber-512, Kyber-768 and Kyber-1024) with four NTT PR bitstreams. In Kyber variants, the parameter n (number of coefficients) is 256, and the modulus q is 3329. Each coefficient requires 12 bits, so the size of the *poly_mem* memory is 12×256 . The *w_mem* memory, which stores the twiddle factors, is also 12×256 .

Both the NTT and the entire Kyber implementation run at a 100 MHz clock frequency. We assume a system setup consisting of an Intel i5 host CPU and an Artix-7 FPGA, which together act as a server platform. In this scenario, the server is expected to execute the Kyber Key Generation, Encapsulation, and Decapsulation processes multiple times, as would be required in practical secure communication applications.

During Kyber's *Key Generation, Encapsulation, and Decapsulation* processes, each NTT operation requires 1024 clock cycles. To emulate the faults caused by a hardware Trojan, we designed a fault injector. This block generates a 10-bit output named as F_r , which is connected to the ten *AND* signals of our **Secure NTT** listed in the 2nd column of Table I. The 10-bit F_r from the fault injector determines whether the actual values of the corresponding signals in Table I are passed to the NTT or blocked. As shown in Fig. 9, instead of using *rd_en* directly to read the polynomial memory, the system uses $F_r[0] \text{ AND } rd_en$. A similar modification is applied to the other nine control signals. We generated two random numbers using the special device file */dev/urandom* available in our Ubuntu host CPU. These two random numbers, named as R_t and R_s are sent to the fault injector through PCI bus. The first random number R_t , selected in the range [0, 1023], determines the specific clock cycle at which the attack is performed on our NTT. The second random number R_s , also in the range [0, 1023], is used to feed the 10-bit output F_r of our fault injector, which specifies the control signal to be compromised. For example, if $R_t = 1002$ and $R_s = 766$, then after the activation of our **Secure NTT**, at the 1002nd clock cycle, the value of R_s will be loaded at the injector output F_r . In this case, $F_r = 1011111110$, which means that the actual values of *rd_en* and *uv_rst* will not be blocked by our fault injector. Therefore, in our fault emulation process, at a random clock cycle of the NTT, we tamper with the control signals of the NTT, which emulates the behavior of a hardware Trojan attack. As shown in Table II, we have run the Kyber Key Generation, Encapsulation, and Decapsulation processes 4096 times. Since each of the three Kyber processes (Key Generation, Encapsulation, and Decapsulation) requires multiple executions of the NTT/INTT, the total number of NTT/INTT operations depends on the specific Kyber variant. For Kyber-512, Kyber-768, and Kyber-1024, we executed our **Secure NTT** implementation 69,632, 98,304, and 1,26,976 times, respectively. In each of these runs, for the entire 1024 clock cycles of NTT activation period, we targeted a specific clock cycle (denoted by R_t) and performed 'Stuck-at-1' and 'Stuck-at-0' attacks on random control signals selected through R_s . As shown in Table II, 100% of the faults emulated by our fault injector are detected by *CFI* and *CCC*, and all detected faults are successfully corrected by our adaptive fault-correction module. For Kyber-512, Kyber-768, and Kyber-1024, we use eight NTT PR bitstreams with eight different slice ranges specified in the Xilinx Design Constraints (XDC)

Block	Sample Size	Kyber-512			Kyber-768			Kyber-1024		
		#NTT Run / Block	Total # NTT Runs & # Faults Injected	Detection & Correction Eff. (%)	#NTT Run / Block	Total # NTT Runs & # Faults Injected	Detection & Correction Eff. (%)	#NTT Run / Block	Total # NTT Runs & # Faults Injected	Detection & Correction Eff. (%)
KeyGen	4096	2	8192	100	3	12288	100	4	16384	100
		2	8192	100	3	12288	100	4	16384	100
		0	0	100	0	0	100	0	0	100
Encap	4096	2	8192	100	3	12288	100	4	16384	100
		2	8192	100	3	12288	100	4	16384	100
		1	4096	100	1	4096	100	1	4096	100
Decap	4096	2	8192	100	3	12288	100	4	16384	100
		2	8192	100	3	12288	100	4	16384	100
		2	8192	100	3	12288	100	4	16384	100
		1	4096	100	1	4096	100	1	4096	100
		1	4096	100	1	4096	100	1	4096	100
Total	12,288	17	69,632	100	24	98,304	100	31	1,26,976	100

TABLE II: Fault Detection and Correction Efficiency for Emulated Faults by Our Fault Injector for Kyber Variants

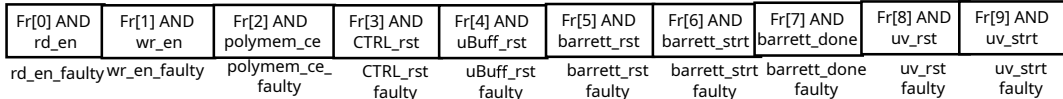


Fig. 9: Connection of Fault Injector with Control Signals

file. The four threshold values are set to $cfi_th_reld = 256$, $cfi_th_relc = 512$, $ccc_th_reld = 256$, and $ccc_th_relc = 512$. The source code of our NTT is available on GitHub¹.

B. Overheads

Table IV shows that the implementation of our proposed fault detection modules, Secure NTT [as per Kyber specifications: $n=256$, $q=3329$], incurs an 8.7% slice overhead and a 2% energy overhead compared to the baseline NTT. It does not cause any timing overhead. The proposed adaptive fault correction scheme and fault detection modules incur a 19.7% slice overhead and a 3% energy overhead compared to the baseline NTT. The timing overhead of the fault correction module depends on the types of measures. For measure III-A1, the overhead is limited to a single clock period of the NTT engine (10 ns in the present configuration), and the R_i update is performed on the host CPU. Because the update runs on the host and the NTT computation continues on dedicated hardware, the host-side R_i update does not affect the executing NTT pipeline. For measure III-A2, the time overhead is dominated by two factors: (i) Time required for R_i update within the bit patcher logic, and (ii) Time to stream the corresponding PR bitstream through the ICAP. For a PR bitstream file of approximately 56 kB NTT, the ICAP transfer requires on the order of $\sim 150 \mu s$ with a 100 MHz ICAP clock and 32-bit data width. This value represents the raw transfer time and excludes any additional protocol framing or controller overhead. For measure III-A3, the time overhead is dominated by three factors: (i) Time required for R_i update within the bit patcher logic, and (ii) PR bitstream configuration time by ICAP and (iii) Time to

choose the PR bit stream based R_i , which takes around $\sim 256 \mu s$.

C. Different Hardware Trojan Scenarios

As shown in Table III, for our Secure NTT, we consider four scenarios based on possible hardware Trojan locations in the system: Outside Upstream, Inside NTT, Outside Downstream, and Inside Monitors. We also consider four different phases of hardware Trojan insertion in the FPGA: RTL, Synthesis/Foundry, Bitstream level, and Post-deployment. Based on the literature, it can be concluded that at the RTL and Synthesis/Foundry phases, all four Trojan locations are possible. At the Bitstream level, attacks on Outside Upstream/Downstream and fault-detection modules are feasible, while Inside-core attacks are harder but still possible. In the Post-deployment phase, only Outside Upstream/Downstream attacks are realistic. Table III illustrates how the location of a hardware Trojan impacts our *CFI*, *CCC*, and *LM*.

1) *Outside Upstream* [23]: Outside upstream means the hardware Trojan is placed on the control signals before they reach the NTT or target core. In our case, the Trojan might be inserted into the data signals coming from *poly_mem* ($A[k0], A[k1]$) or from *w_mem* (w_j). These types of Trojans can perform a SASCA-style attack through raw inputs. However, the data signals in the first NTT iteration may arrive without masking, while all subsequent outputs ($U+V$ and $U-V$) stored in *poly_mem* are written after masking using our *LM* circuit. Therefore, during the entire NTT activation period, the probability of SASCA-style leakage is only 1/1024 in our Kyber implementation, whereas for the unprotected existing NTT it is 1. Pre-masking taps or removal of masking are also not possible at the outside bitstream level, since the *LM* is placed inside the NTT.

¹https://github.com/rourabpaul1986/NTT/tree/master/fntt_pipelined

2) *Inside NTT/Target Core* [24]: The Trojan is embedded within the NTT itself, directly manipulating its internal signals, operations such as butterfly units, modular reductions, or memory accesses. In our NTT, if a hardware Trojan is inserted within the NTT itself and possibly introduced through compromised synthesis or foundry stages [11], control-flow hijacking or trigger-based payloads are effectively detected by *CFI*, while Trojan-induced delays are reliably detected by *CCC*.

3) *Outside-Downstream* [25]: The Trojan resides after the NTT output, i.e., outside the NTT block, and manipulates or taps the results before they are consumed by subsequent cryptographic operations. A SASCA type leakage through output tapping is not effective because the two output signals of our NTT, $U + V$ and $U - V$, are always masked by the *LM*. Furthermore, output manipulation in this case does not fall under control signal attacks, and is therefore considered out of scope.

4) *Inside Monitors* [25]: Another possible scenario arises when the hardware Trojan is inserted inside the fault detection module itself. In our case, if the Trojan compromises either the *CCC* or *CFI*, the system may fail to detect faults accurately, potentially leading to overall failure of our *Secure NTT*.

D. Comparison with Existing Works

In the literature, many NTT implementations exist. Based on fault detection characteristics, they can be categorized into two types: those focusing on data-signal fault detection [17], [19], and those focusing on control-signal fault detection [5], [7], [8]. Since faults on NTT data signals are beyond the scope of this paper, we restrict our comparison to works that focus specifically on NTT control signals. Jati et al. [5] implement an NTT on an Artix-7 FPGA using Random Access Memory and a Clock Cycle Counter (*CCC*) to prevent SASCA and unconventional delays. Ravi et al. [7] and Rafael et al. [8] both apply local masking to polynomial coefficients to protect the NTT from SASCA. The key difference is that [7] employs randomly accessible polynomial coefficient memory, which provides additional protection against SCAs. In our fault detection methodology, we adopt existing techniques such as local masking and the clock cycle counter, but additionally introduce a lightweight shift-register-based backup CSR that is fully independent of the NTT. This fault detection modules imposes only 8.7% slice overhead and a 2% energy overhead compared to the baseline NTT. It does not cause any timing overhead. Our *Secure NTT* also implements adaptive fault correction methods with three different measures : III-A1, III-A2 and III-A3. The proposed adaptive fault-correction and fault-detection modules impose a combined resource overhead of 19.7% in slices and an energy overhead of 3% relative to the baseline. The timing overhead varies with the specific measurement method; details are provided in Sec. IV-B. These overheads are tolerable in practical implementations of NTT, as used in Kyber, Dilithium, and other lattice-

based cryptographic algorithms. As shown in Table V, we compare our adaptive fault-correction approach with existing PR-based fault-correction techniques. While existing fault correction solutions focus mainly on recovering from configuration or memory upsets with large area or timing penalties, our design uniquely targets control signal faults induced by hardware Trojans and side-channel conditions. The results demonstrate that the overhead introduced by our method remains reasonable compared with current systems. To the best of our knowledge, this is the first fault-correction strategy that adapts its behavior to the nature of the fault itself.

V. CONCLUSION

In this paper, we propose a *Secure NTT* architecture that detects faults using two key techniques: (i) a shift-register-based lightweight backup control status register to ensure control-flow integrity, and (ii) a clock-cycle counter applied to all critical signals to detect unconventional delays. In addition, a local masking scheme is employed to prevent side-channel attacks such as SASCA. Together, these measures prevent control-flow disruptions, hardware Trojan induced delays in subcomponents, and side-channel leakages. We also implement an adaptive fault-correction module for our *Secure NTT*, tailored to the specific fault types caused by hardware Trojans. Our results shows implementation cost of the above mentioned measures in our *Secure NTT* is nominal and competitive with the existing NTTs.

VI. FUTURE SCOPE

The proposed fault detection technique is highly logic-specific to the NTT algorithm; however, the adaptive fault correction methods can also be applied to other critical modules of lattice-based PQC algorithms. In the future, we plan to implement a PQC security processor integrating Kyber for public-key encryption, Dilithium for digital signatures, and AES-256 for symmetric-key encryption. In this security processor, different fault detection modules will be adopted for the critical components of Kyber, Dilithium, and AES—such as Noise Sampling, KECCAK, Matrix–Vector Multiplication, S-Box, ShiftRows, MixColumns, etc.—while all components will share the same adaptive fault correction mechanism as proposed here.

Acknowledgment This publication has emanated from research conducted with the financial support of Taighde Éireann - Research Ireland under Grant number 13/RC/2077_P2 at CONNECT: the Research Ireland Centre for Future Networks.

REFERENCES

- [1] Li et al. Reconfigurable and high-efficiency polynomial multiplication accelerator for crystals-kyber. *IEEE Transactions on Computer-Aided Design of Integrated Circuits and Systems*, 42(8):2540–2551, 2023.
- [2] Bin Li, Yunfei Yan, Yuanxin Wei, and Heru Han. Scalable and parallel optimization of the number theoretic

TABLE III: Trojan Scenarios for NTT with Local Mask (LM) Unit, Control-Flow Integrity (CFI) Checker, and Clock Cycle Counter (CCC)

Trojan Location	Trojan Type / Payload	Insertion Phase	Impact on NTT	LM	CFI	CCC	Remarks
Outside Upstream [23]	SASCA-style leakage via raw inputs	Post-deployment [26] / side-channel [7], [8]	Secret key/ plaintext leakage	✓	✗	✗	Input data of NTT is masked by ω_r in LM
	Pre-mask tap (copies inputs before masking)	RTL / synthesis	Secret leakage (mask bypass)	✗	✗	✗	Not possible as LM is placed inside NTT
	Clock glitch/ insertion, Reset spoofing, DoS, loss of state	Post-deployment [26] / fault injection	Integrity fault, timing errors	✗	~	~	Trojan in the NTT main clk or rst introduces ambiguity in control flow and may cause delays, which can be detected by CSR and CCC respectively
Inside NTT [24]	Data leak after mask removal (tap internal nets)	RTL [10] / synthesis [11]	Secret leakage inside datapath	✗	✗	✗	If a hardware Trojan inside the NTT removes LM, the attack directly disables a critical functionality of the design. Since the LM has no explicit control pins to manipulate, such an attack cannot be classified as a control-signal attack; rather, it constitutes a payload-level functional disruption Trojan.
	Control-flow hijack (illegal state/branch)	RTL [10] / synthesis [11]	Integrity violation, wrong outputs	✗	✓	~	Independent shift registers (CSR) inside CFI mimic NTT's control flow; deviations indicate a Trojan. If timing delays in NTT subcomponents (read, write, Barrett, etc.) are detected by CCC
	Trigger-based payload (rare sequence)	RTL [10] / synthesis [11]	Conditional leakage or DoS	✗	✓	~	If a conditionally activated Trojan alters control flow or delays NTT sub-components, both CSR and CCC can detect it for the reasons stated above
	Timing/ delay Trojan (extra states, gated clock)	RTL [10] / synthesis [11]	DoS or covert timing side channel	✗	~	✓	If the Trojan is covert but adds extra states or a gated clock, causing NTT stalling or delays, it can be detected by CCC and CFI.
Outside Downstream [25]	Output manipulation exfiltration (covert I/O pin, encoding)	RTL [10] / synthesis [11]	Secret leakage via outputs	✗	✗	✗	It's not control-signal attacks, and is therefore considered out of scope.
	SASCA-style leakage via raw outputs	RTL [10] / synthesis [11]	Secret leakage via outputs	~	✗	✗	During the entire NTT operation and subsequent Kyber/Dilithium processing, inputs remain masked and are only unmasked after the inverse NTT (INTT). If output exfiltration occurs after INTT, it cannot be protected by LM; otherwise, any leakage before INTT can be mitigated by LM
Inside monitors [25]	Trojan in CFI (forces "pass")	RTL [10] / synthesis [11]	Integrity violation undetected (I)	✗	Tampered	~	CFI Compromized
	Trojan in counter (forges/freeze count)	RTL [10] / synthesis [11]	Timing deviations undetected	✗	~	Tampered	CCC Compromized

transform based on fpga. *IEEE Transactions on Very Large Scale Integration (VLSI) Systems*, 32(2):291–304, 2024.

- [3] Ahmet Can Mert, Emre Karabulut, Erdinç Öztürk, Erkay Savaş, and Aydin Aysu. An extensive study of flexible design methods for the number theoretic transform. *IEEE Transactions on Computers*, 71(11):2829–2843, 2022.
- [4] Robert Primas, Peter Pessl, and Stefan Mangard.

Single-trace side-channel attacks on masked lattice-based encryption. In *Cryptographic Hardware and Embedded Systems – CHES 2017*, pages 513–533, Cham, 2017. Springer International Publishing.

- [5] Arpan Jati, Naina Gupta, Anupam Chattopadhyay, and Somitra Kumar Sanadhya. A configurable crystals-kyber hardware implementation with side-channel protection. *ACM Trans. Embed. Comput. Syst.*, 23(2), March 2024.

Designs	Platform	# of Butterfly Unit	SEC*	BRAM	Energy	CCs	Protection	Prevent
[5]	Artix-7 FPGA	1	280	1	NR	570	Random Memory Access, Clock Cycle Count	SASCA, Unconventional
[7]	ARM Cortex M4	-	-	-	NR	178×10^3	Local Masking, Random Memory Access	SASCA
[8]	Artix-7 FPGA	4	1492	6	NR	237	Partial Local Masking	SASCA
Ours baseline	Artix-7 FPGA	1	273	1	2991 nJ	1028	Nil	Nil
Ours protected (only detection)	Artix-7 FPGA	1	297 (↑8.7%)	1	3021 nJ (↑1%)	1028 (0%)	Back up & Independent CSR, Local Masking, Clock Cycle Counter	<i>CFI</i> , Delays, SASCA
Ours protected (detection+correction)	Artix-7 FPGA	1	327 (↑19.7%)	1	3094 nJ (↑3.%)	1028 + BitPatch Time	Back up & Independent CSR, Local Masking, Clock Cycle Counter, Adaptive Fault Correction	<i>CFI</i> , Unconventional Delays, SASCA

* Slice Eq. Cost(SEC)=LUTs×0.25 + FFs×0.25 + DSPs×100 [27]. NR: Not Reported

TABLE IV: Comparison of Overhead & Threat Protection of Our NTT with Other Control-Signal-Based Protections

Works	FPGA	Application	Target	Correction Technique	Overheads
[28]	Xilinx Zynq-7000	Secure crypto IP updates	Crypto module bit-streams	PR with Authenticated Encryption with Associated Data (AEAD) authentication using PUF-derived keys	~7–10% area increase for PR controller; negligible time overhead during normal operation
[29]	Xilinx Kintex-7	FFT processors (analogous to NTT)	Faulty FFT cores due to SEUs	PR to replace faulty cores (on-demand scrubbing)	Recovery latency per core swap ≈ 20–50 ms; area overhead for spare logic ≈ 5–8%
[30]	Generic Xilinx FPGA	Radiation-prone environments, e.g., space	Fault tolerance for FPGA-based systems under SEUs (Single Event Upsets)	Fault detection with TMR + diagnostic logic, partial dynamic reconfiguration of only the faulty module via a Reconfiguration Controller	Simulation-based; no measured slice or energy overheads reported. Reliability evaluated as a function of reconfiguration time. Controller includes minor logic for partial reconfiguration.
[31]	Generic FPGA	Reconfiguration security (DPA attack countermeasures)	PR controller logic	PR with ReCoFuse container for formal violation detection	9% LUT increase, 6% FF increase reported; reconfiguration time 30 ms per region
[32]	Modern SRAM-based FPGAs	Safety-critical dynamically & PR systems (e.g., space, avionics)	Single and multiple errors caused by harsh conditions (SEUs)	Self-repairing method using run-time partial and dynamic reconfiguration at fine-grain granularity	TMR consumes on average 3.64× more hardware resources than the original circuit.
[33]	SRAM-based FPGAs	FPGA lifetime extension under permanent SEE (space missions)	Permanent config faults (SEEs)	PR deleting faulty frames; scrubbing only faulty frames	Extends device lifetime significantly; reduced reconfiguration traffic vs full scrubbing (quantitative area/time overhead not detailed)
Our	Artix-7	NTT, Security Processor	Faults in control signals caused by hardware Trojans & SCA	Depending on control signal faults, adaptive fault correction	10.1% slice, 1% energy increase; time depends on nature of faults(stated in IV-B)

TABLE V: FPGA Partial Reconfiguration in Fault-Correction

[6] Samaneh Ghandali, Thorben Moos, Amir Moradi, and Christof Paar. Side-channel hardware trojan for provably-secure sca-protected implementations. *IEEE Transactions on Very Large Scale Integration (VLSI) Systems*, 28(6):1435–1448, 2020.

[7] Prasanna Ravi, Romain Poussier, Shivam Bhasin, and Anupam Chattopadhyay. On configurable sca countermeasures against single trace attacks for the ntt: A performance evaluation study over kyber and dilithium on the arm cortex-m4. In *Proceedings of the International Conference on Cryptographic Hardware and Embedded Systems*, page 123–146, Berlin, Heidelberg, 2020. Springer-Verlag.

[8] Rafael Carrera Rodriguez, Emanuele Valea, Florent Bruguier, and Pascal Benoit. Hardware implementation and security analysis of local-masked NTT for CRYSTALS-kyber. Cryptology ePrint Archive, Paper 2024/1194, 2024.

[9] Mordor Intelligence. Field programmable gate array market size & share analysis – growth trends & forecasts (2025–2030). Mordor Intelligence Industry Report, 2025. Market size: USD 10.08 billion (2025), projected to expand to USD 16.23 billion by 2030 at 10.00% CAGR.

[10] Ruochen Dai, Zhaoxiang Liu, Orlando Arias, Xiaolong Guo, and Tuba Yavuz. Dtjrtl: A configurable frame-

work for automated hardware trojan insertion at rtl. In *Proceedings of the Great Lakes Symposium on VLSI 2024*, GLSVLSI '24, page 465–470, New York, NY, USA, 2024. Association for Computing Machinery.

[11] Rijoy Mukherjee, Archisman Ghosh, and Rajat Subhra Chakraborty. Hls-irt: Hardware trojan insertion through modification of intermediate representation during high-level synthesis. *ACM Trans. Des. Autom. Electron. Syst.*, 29(5), September 2024.

[12] Paweł Swierczynski, Marc Fyrbik, Philipp Koppe, and Christof Paar. Fpga trojans through detecting and weakening of cryptographic primitives. *IEEE Transactions on Computer-Aided Design of Integrated Circuits and Systems*, 34(8):1236–1249, 2015.

[13] Tony F. Wu, Karthik Ganesan, Yunqing Alexander Hu, H.-S. Philip Wong, Simon Wong, and Subhasish Mitra. Tpad: Hardware trojan prevention and detection for trusted integrated circuits. *Trans. Comp.-Aided Des. Integ. Cir. Sys.*, 35(4):521–534, April 2016.

[14] Zhiming Zhang, Laurent Njilla, Charles A. Kamhoua, and Qiaoyan Yu. Thwarting security threats from malicious fpga tools with novel fpga-oriented moving target defense. *IEEE Transactions on Very Large Scale Integration (VLSI) Systems*, 27(3):665–678, 2019.

[15] Kanad Basu, Samah Mohamed Saeed, Christian Pilato, Mohammed Ashraf, Mohammed Thari Nabeel, Krishnendu Chakrabarty, and Ramesh Karri. Cad-base: An attack vector into the electronics supply chain. *ACM Trans. Des. Autom. Electron. Syst.*, 24(4), April 2019.

[16] Ausmita et al., Sarker and Canto. Error detection architectures for hardware/software co-design approaches of number-theoretic transform. *IEEE Transactions on Computer-Aided Design of Integrated Circuits and Systems*, 42(7):2418–2422, 2023.

[17] Rourab Paul, Paresh Baidya, and Krishnendu Guha. Lightweight fault detection architecture for ntt on fpga, 2025.

[18] Saeed Aghapour, Kasra Ahmadi, Mehran Mozaffari Kermani, and Reza Azarderakhsh. Partial recomputation fault detection architecture for multiple-precision montgomery modular multiplication. *IEEE Transactions on Computer-Aided Design of Integrated Circuits and Systems*, pages 1–1, 2025.

[19] Sven Bauer, Fabrizio De Santis, Kristjane Koleci, and Anita Aghaie. A fault-resistant NTT by polynomial evaluation and interpolation. *Cryptology ePrint Archive*, Paper 2024/788, 2024.

[20] Prasanna et al. Generic side-channel attacks on cca-secure lattice-based pke and kems. *IACR Transactions on Cryptographic Hardware and Embedded Systems*, 2020(3):307–335, Jun. 2020.

[21] Alban Bourge, Olivier Muller, and Frédéric Rousseau. Generating efficient context-switch capable circuits through autonomous design flow. *ACM Trans. Reconfigurable Technol. Syst.*, 10(1), December 2016.

[22] Xilinx, Inc. *Vivado Design Suite User Guide: Partial Reconfiguration (UG909)*, 2015. Version 2015.4; Xilinx Vivado.

[23] Burin Amornpaisanon, Andreas Diavastos, Li-Shiuan Peh, and Trevor E. Carlson. Secure run-time hardware trojan detection using lightweight analytical models. *Trans. Comp.-Aided Des. Integ. Cir. Sys.*, 43(2):431–441, February 2024.

[24] Athanasios Moschos, Fabian Monroe, and Angelos D. Keromytis. Towards practical fabrication stage attacks using interrupt-resilient hardware trojans. In *2024 IEEE International Symposium on Hardware Oriented Security and Trust (HOST)*, pages 254–259, 2024.

[25] Kevin Immanuel Gubbi, Banafsheh Saber Latibari, Anirudh Srikanth, Tyler Sheaves, Sayed Arash Beheshti-Shirazi, Sai Manoj PD, Satareh Rafatirad, Avesta Sasan, Houman Homayoun, and Soheil Salehi. Hardware trojan detection using machine learning: A tutorial. *ACM Trans. Embed. Comput. Syst.*, 22(3), April 2023.

[26] Qazi Arbab Ahmed, Tobias Wiersema, and Marco Platzner. Post-configuration activation of hardware trojans in fpgas. *Journal of Hardware and Systems Security*, 8(2):79–93, 2024.

[27] Liu et al. Optimized schoolbook polynomial multiplication for compact lattice-based cryptography on fpga. *IEEE Transactions on Very Large Scale Integration (VLSI) Systems*, 27(10):2459–2463, 2019.

[28] Manuel Unterstein, Arne Schäffers, Maksym Skorobogatyi, Anh Dang, Felix Stumpf, and Axel Poschmann. Secure update of fpga-based secure elements using partial reconfiguration. Technical Report 2020/833, IACR ePrint Archive, 2020.

[29] Xin Wei, Yi Z Xie, Yu Xie, and He Chen. Dynamic partial reconfiguration scheme for fault-tolerant fft processor based on fpga. *The Journal of Engineering*, 2019:7424–7427, 2019.

[30] Richard Panek, Jakub Lojda, Jakub Podivinsky, and Zdenek Kotasek. Partial dynamic reconfiguration in an fpga-based fault-tolerant system: Simulation-based evaluation. In *2018 IEEE East-West Design & Test Symposium (EWDTS)*, pages 1–6, 2018.

[31] Buse Ustaoglu, Kenneth Schmitz, Daniel Große, and Rolf Drechsler. Recofused partial reconfiguration for secure moving-target countermeasures on fpgas. *SN Applied Sciences*, 2:1363, 2020.

[32] Matteo Sonza Reorda, Luca Sterpone, and Anees Ullah. An error-detection and self-repairing method for dynamically and partially reconfigurable systems. *IEEE Transactions on Computers*, 66(6):1022–1033, 2017.

[33] Jose Luna, Luis Entrena, Mario Garcia-Valderas, and Celia Lopez-Ongil. Optimal partial reconfiguration for permanent fault recovery on sram-based fpgas. *ISRN Electronics*, 2013:Article ID 783673, 2013.